Springer

KSME

Journal of Mechanical Science and Technology 24 (11) (2010) 2221~2232
www.springerlink.com/content/1738-494x
DOI 10.1007/s12206-010-0817-2

Creep modeling in functionally graded rotating disc of variable thickness †

D. Deepak[1], V. K. Gupta[2,*] and A. K. Dham[3]

[1]*Department of Mechanical Engg., R.I.E.I.T.,Railmajra, 144533, India*
[2]*Mech. Engg., UCoE, Punjabi University, Patiala-147002, India*
[3]*Department of Physics, Punjabi University, Patiala-147002, India*

(Manuscript Received July 21, 2009; Revised May 30, 2010; Accepted July 27, 2010)

Abstract

Creep behavior of rotating discs made of functionally graded materials with linearly varying thickness has been investigated. The discs under investigation are made of composite containing silicon carbide particles in a matrix of pure aluminum. The creep behavior of the composite has been described by threshold stress based creep law by assuming a stress exponent of 5. The effect of imposing linear particle gradient on the distribution of stresses and strain rates in the composite disc has been investigated. The study indicates that with increase in particle gradient in the disc, the radial stress increases throughout the disc, whereas the tangential and effective stresses increase near the inner radius but decrease near the outer radius. The steady state strain rates in the composite disc, having gradient in the distribution of reinforcement, are significantly lower than that observed in a disc having uniform distribution of reinforcement.

Keywords: Functionally graded material; Modeling; Rotating disc; Steady state creep

1. Introduction

Rotating discs provide an area of research and study due to their vast utilization in rotating machinery such as steam and gas turbine rotors, turbo generators, pumps, compressors, flywheels, automotive braking systems, ship propellers and computer disc drives [1-4]. In most of these applications, the disc has to operate under elevated temperature and is simultaneously subjected to high stresses caused by disc rotation at high speed [5]. As a result of severe mechanical and thermal loadings, the material of disc undergoes creep deformations, thereby affecting performance of the system [1, 6-8]. As an example, in the turbine rotor, there is always a possibility that the heat from the external surface is transmitted to the shaft and then to the bearings, which has adverse effects on the functioning and efficiency of the rotor [9].

Under high temperature, a rotating disc made of monolithic material may not perform well. The excellent mechanical properties like high specific strength and stiffness, and high temperature stability offered by aluminum matrix composites reinforced with SiC particles, whiskers or fibers make them suitable for rotating disc applications exposed to elevated temperature [10-11].

In recent years, the problem of creep in rotating discs made of functionally graded materials (FGMs), subjected to severe mechanical and thermal loads, has attracted the interest of many researchers. In FGMs the volume fraction of one or more constituent material is varied continuously as a function of position along certain dimension(s) [12, 13]. These materials are designed and developed to operate in high temperature environments. The steady state creep behavior of a rotating disc made of functionally graded (FG) isotropic Al-SiCp (subscript 'p' for particle) having constant thickness and operating under constant temperature was studied by Singh and Ray [14]. The study assumed linearly decreasing distribution of SiCp from the inner to the outer radius of disc. It is revealed that the steady state creep response of FGM disc is significantly superior as compared to a similar disc but containing uniform distribution of SiCp. Gupta et al. [1, 15] analyzed creep behavior of a rotating disc made of FG Al-SiCp having uniform thickness and operating under a radial thermal gradient. The study indicates that for the assumed linear distribution of SiCp, the steady-state strain rates in an FGM disc are significantly lower than that observed in an isotropic disc having uniform distribution of SiCp. Bayat et al. [16] carried out thermo-elastic analysis of an FG rotating disc with small and large deflections and observed that for particular values of grading index (n) of material properties mechanical responses in FG disc can be smaller than observed in a homogeneous disc. Bayat et al. [9] obtained elastic solutions for axisymmetric rotating discs made of FGM with variable thickness. Kordkheili and Naghdabadi [17] obtained a semi-analytical

† This paper was recommended for publication in revised form by Associate Editor Seong Beom Lee

* Corresponding author. Tel.: +91 175 2280166, Fax: +91 175 3046333
E-mail address: guptavk_70@yahoo.co.in

thermo-elastic solution for hollow and solid rotating axisymmetric disc made of FGM under plane stress condition.

The literature reveals that the stresses in rotating discs (annular or solid) having variable thickness, with thickness decreasing from the center towards the periphery, are much lower than those observed in a uniform-thickness disc operating at the same angular velocity [18-20]. By employing a variable thickness disc the plastic limit angular velocity increases and the magnitude of stresses and deformations in the disc reduces [20]. Jahed et al. [21] observed that the use of variable thickness disc helps in minimizing the weight of disc in aerospace applications. Gupta et al. [22] also observed that a rotating disc whose density and thickness decrease radially is on the safer side of design in comparison to a flat disc having variable density. Deepak et al. [23] noticed that the stresses and strain rates in a rotating disc made of isotropic composite can be significantly reduced by selecting linearly varying thickness profile as compared to hyperbolic or constant thickness disc profile.

The literature consulted so far reveals that the studies pertaining to creep in rotating disc made of FGM, that too of variable thickness, are rather scant. Further, the creep performance of composite disc with linearly varying thickness is observed to be superior as compared to discs having other thickness profiles. With these forethoughts, it is decided to investigate the steady state creep, which occupies 30-40% of total creep life, in a rotating disc made of functionally graded Al-SiCp and having linearly varying thickness. The content of SiCp in Al matrix is assumed to vary linearly with maximum SiCp content at the inner radius and minimum SiCp content at the outer radius. A mathematical model has been developed to describe the steady creep behavior of the composite disc. The model is used to investigate the effect of imposing various kinds of linear particle (SiCp) gradients on the steady state creep response of a variable thickness disc.

2. Disc profile and assumptions

In this study, the creep response has been calculated for rotating discs having linearly varying thickness and constant thickness while keeping equal volume of both the disc. The inner (a) and outer (b) radii of both the discs are assumed, respectively, as 31.75 *mm* and 152.4 *mm* while the thickness (t) of uniform thickness disc is taken as 25.4 *mm.* The dimensions of the disc selected in this study are similar to those reported earlier [18].

In case of linearly varying thickness disc, the thickness $h(r)$ at any radius r is given by

$$h(r) = h_b + 2c(b - r)\,, \tag{1}$$

where the constant $c = \dfrac{(h_a - h_b)}{2(b-a)}$, and h_a and h_b are, respectively, the disc thickness at $r = a$ and $r = b$.

Since the volume of linearly varying thickness disc is equal to that of constant thickness disc,

$$\int_a^b 2\pi r h(r)\,dr = \pi(b^2 - a^2)t\,. \tag{2}$$

Substituting $h(r)$ from Eq. (1) into the above equation and simplifying, we get,

$$h_a = \frac{3(b+a)t - h_b(2b+a)}{(b+2a)}\,. \tag{3}$$

Assuming h_b =13.97 *mm* and substituting a = 31.75 *mm*, b = 152.4 *mm* and t = 25.4 *mm* in Eq. (3), we get h_a = 43.22 *mm.*

The analysis carried out in this study is based on the following assumptions:

(1) Material of the disc is incompressible and locally isotropic, i.e., the properties of the disc remain constant at a given radius in all the directions but change with the change in radius.
(2) Stresses at any point in the disc remain constant with time, *i.e.,* steady state condition of stress is assumed.
(3) Elastic deformations in the disc are small and neglected as compared to creep deformations.
(4) The axial stress (σ_z) throughout the disc remains zero.

3. Distribution of reinforcement

The distribution of SiCp in the FGM disc decreases linearly from the inner to outer radius; therefore, the density and the creep constants will also vary with radial distance. The amount (*vol%*) of SiCp, $V(r)$, at any radius r, is given by

$$V(r) = V_{\max} - \frac{(r-a)}{(b-a)}(V_{\max} - V_{\min}) = \delta_1 - \delta_2 r\,, \tag{4}$$

where

$$\delta_1 = (V_{\max} + a\delta_2)\,,$$
$$\delta_2 = \frac{(V_{\max} - V_{\min})}{(b-a)}\,.$$

$V_{\max}$ and $V_{\min}$ are the maximum and minimum SiCp contents, respectively, at the inner (a) and the outer (b) radius of the disc.

According to rule of mixture, the density $\rho(r)$ of the FGM disc at any radius r may be written as,

$$\rho(r) = \frac{[100 - V(r)]\rho_m + V(r)\rho_d}{100} = \rho_m + \frac{(\rho_d - \rho_m)V(r)}{100}\,, \tag{5}$$

where, ρ_m (= 2698.9 *kg/m*^{3}) and ρ_d (= 3210 *kg/m*^{3}) are,

respectively, the densities of pure aluminum matrix and silicon carbide particles [24, 25].

Substituting $V(r)$ from Eq. (4) into Eq. (5),

$$\rho(r) = \rho_m + \frac{(\rho_d - \rho_m)(\delta_1 - \delta_2 .r)}{100} = A_\rho - B_\rho .r \,, \tag{6}$$

where,

$$A_\rho = \rho_m + (\rho_d - \rho_m)\frac{\delta_1}{100} .$$

and,

$$B_\rho = \frac{\delta_2(\rho_d - \rho_m)}{100} .$$

The average particle content in the disc (V_{av}) can be expressed as,

$$V_{av} = \frac{\int_a^b 2\pi r h(r) V(r) dr}{\pi(b^2 - a^2)t} . \tag{7}$$

Substituting $h(r)$ and $V(r)$, respectively, from Eq. (1) and Eq. (4) into Eq. (7), the minimum SiCp content (V_{min}) in the disc may be obtained as,

$$V_{\min} = \frac{V_{\max}(h_b b^2 - 2h_b a^2 + b^3 c - 5a^2 bc + ab^2 c + ab h_b + 3a^3 c) - 3V_{av} t(b^2 - a^2)}{(abh_b + ab^2 c + a^2 h_b + a^2 bc - a^3 c - 2b^2 h_b - b^3 c)} \tag{8}$$

4. Selection of creep law

In aluminum-based composites, undergoing steady state creep, the effective creep rate ($\dot{\bar{\varepsilon}}$) is related to the effective stress ($\bar{\sigma}$) through well documented creep law given by [26, 27]:

$$\dot{\bar{\varepsilon}} = A'\left(\frac{\bar{\sigma} - \sigma_0(r)}{E}\right)^n \exp\left(\frac{-Q}{RT}\right), \tag{9}$$

where the symbols A', n, Q, E, R, T and (σ_0) denote, respectively, the structure dependent parameter, true stress exponent, true activation energy, temperature-dependent Young's modulus, gas constant, operating temperature and threshold stress (i.e., the minimum stress required to initiate creep).

The true stress exponent (n) in Eq. (9) is usually selected as 3, 5 and 8, which correspond to three well-documented creep cases for metals and alloys: (i) n = 3 for creep controlled by viscous glide processes of dislocation, (ii) n = 5 for creep controlled by high temperature dislocation climb (lattice diffusion), and (iii) n = 8 for lattice diffusion-controlled creep with a constant structure [27]. Though, some of the investigators [28-31] have used a true stress exponent of 8 to describe steady state creep in Al-SiCp,w (subscript 'p' for particle and 'w' for whisker) composites but a large number of other investigators [32-39] have suggested that a stress exponent of either ~3 or ~5, rather than 8, provides a better description of experimental steady state creep data observed for discontinuously reinforced Al-SiC composites. As a consequence, a stress exponent of 5 is used in this study to describe steady state creep behavior of the composite discs.

5. Estimation of creep parameters

The creep law given in Eq. (9) may alternatively be written as

$$\dot{\bar{\varepsilon}} = \left[M(r)\left\{\bar{\sigma} - \sigma_0(r)\right\}\right]^n , \tag{10}$$

where $M(r) = \frac{1}{E}\left(A' \exp\frac{-Q}{RT}\right)^{1/n}$ is a creep parameter.

The creep parameters $M(r)$ and $\sigma_0(r)$ given in Eq. (10) are dependent on the type of material and are also affected by the temperature (T) of application. In a composite, the dispersoid size (P) and the content of dispersoid (V) are the primary material variables affecting these parameters. In this study, the values of M and σ_0 have been extracted from the experimental uniaxial creep results reported for Al-SiC_P [30]. For this purpose the individual set of creep data reported in [30] are represented on $\dot{\varepsilon}^{1/5}$ versus σ linear plots as shown in Figs. 1(a)-(c). The slopes and intercepts of these graphs yield the values of creep parameters M and σ_0 as reported in Table 1. This approach of determining the threshold stress (σ_0) is known as linear extrapolation technique [40]. To avoid variation due to systematic error, if any, in the experimental results, the creep results from a single source [30] have been used.

The $\dot{\varepsilon}^{1/5}$ versus σ plots, corresponding to the observed experimental data points of Al- SiC_P [30] for various combinations of SiC_P size, SiC_P content and operating temperature, exhibit an excellent linearity, as evident from Figs. 1(a)-(c). The coefficient of correlation for these plots is observed in excess to 0.916 as evident from Table 1. In the light of these facts, the choice of stress exponent n = 5, to describe the steady state creep behavior of Al-SiC_P, is justified.

For the creep parameters given in Table 1, the regression analysis has been performed in DATAFIT software to estimate the values of M and σ_0 at any radius r of the FGM disc in terms of P, V and T. The developed regression equations are,

$$M(r) = 0.0288 - \frac{0.0088}{P} - \frac{14.0267}{T} - \frac{0.0322}{V(r)} , \tag{11}$$

$$\sigma_0(r) = -0.084P - 0.023T + 1.185V(r) + 22.207 \tag{12}$$

To verify the accuracy of the regression equations developed, the creep parameters corresponding to observed experimental

Table 1. Creep parameters used for Al-SiCp in the present study.

P (μm)	*T* (K)	*V* (vol%)	*M* ($s^{-1/5}$/ *MPa*)	σ_0 (MPa)	Coefficient of Correlation
1.7			4.35E-03	19.83	0.945
14.5	623	10	8.72E-03	16.50	0.999
45.9			9.39E-03	16.29	0.998
		10	4.35E-03	19.83	0.945
1.7	623	20	2.63E-03	32.02	0.995
		30	2.27E-03	42.56	0.945
	623		2.63E-03	32.02	0.995
1.7	673	20	4.14E-03	29.79	0.974
	723		5.92E-03	29.18	0.916

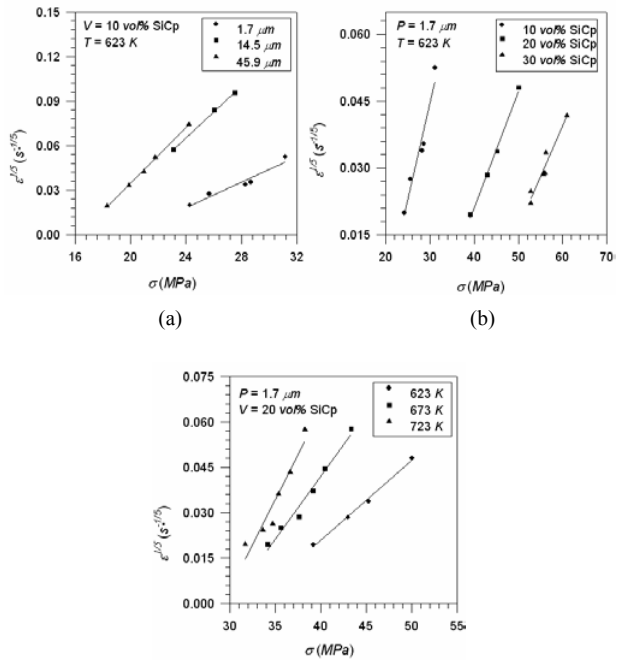

(a) (b)

(c)

Fig. 1. Variation of $\dot{\varepsilon}^{1/5}$ versus σ in Al-SiCp for different: (a) SiCp sizes, (b) *vol %* of SiCp (c) Operating temperatures [30].

data points, as given in Table 1, have been calculated from Eqs. (11) and (12).

The creep parameters thus obtained have been substituted in creep law given by Eq. (10) to estimate the strain rates corresponding to the reported experimental stress levels [30] for various combinations of *P*, *V* and *T*. The strain rates thus estimated have been compared with the experimentally observed strain rates [30] as shown in Figs. 2(a)-(c). An excellent agreement is observed between the theoretical and the experimental strain rates.

In a rotating disc made of FGM, with SiC_P content varying along radius as *V(r),* both the creep parameters *M* and σ_0 will also vary along the radial direction. In the present study, the size of SiC_P (*P*) is taken as 1.7 *μm* and the operating temperature (*T*) is assumed as 623 *K* over the entire disc. Thus, for a given FGM disc with a known particle gradient, both the creep parameters will be functions of radial distance only. The values of *M* (*r*) and $\sigma_0(r)$ at any radius *r*, could be estimated

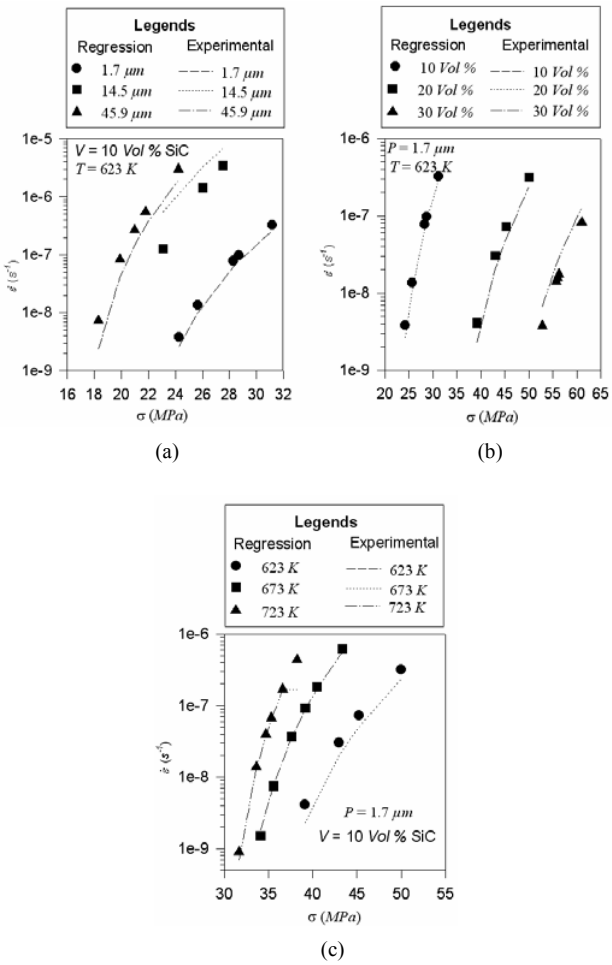

(a) (b)

(c)

Fig. 2. Comparison of experimental [30] and estimated strain rates in Al-SiCp for different: (a) sizes of SiCp, (b) *vol%* of SiCp and (c) Operating temperatures.

by substituting the particle content *V*(*r*) at the corresponding locations into Eqs. (11) and (12) respectively.

6. Mathematical formulation

It is assumed in this study that the disc material is isotropic and yield according to von-Mises yield criterion [41] given by,

$$f(\sigma_{ij}) = J_2 - k^2 = 0 \,, \tag{13}$$

where $f(\sigma_{ij})$ is the potential function, *k* is a constant and J_2 is given by

$$J_2 = \frac{1}{6}[(\sigma_2 - \sigma_3)^2 + (\sigma_3 - \sigma_1)^2 + (\sigma_1 - \sigma_2)^2] \,. \tag{14}$$

The strain increment $(d\varepsilon_{ij})$ is related to the potential function, $f(\sigma_{ij})$, through the associated flow rule given by,

$$d\varepsilon_{ij} = d\lambda \frac{\partial f(\sigma_{ij})}{\partial \sigma_{ij}} \,, \tag{15}$$

where $d\lambda$ is the proportionality factor that depends upon σ_{ij}, $d\sigma_{ij}$ and ε_{ij}, apart from strain history because of strain hardening.

Substituting the yield criterion given by Eq. (13) into Eq. (15), the following constitutive equations are obtained in terms of principal strain increments $d\varepsilon_{11}$, $d\varepsilon_{22}$ and $d\varepsilon_{33}$ and principal stresses σ_{11}, σ_{22} and σ_{33}:

$$\begin{aligned} d\varepsilon_{11} &= \frac{2}{3}\left[\sigma_{11} - \frac{(\sigma_{22}+\sigma_{33})}{2}\right]d\lambda, \\ d\varepsilon_{22} &= \frac{2}{3}\left[\sigma_{22} - \frac{(\sigma_{11}+\sigma_{33})}{2}\right]d\lambda, \\ d\varepsilon_{33} &= \frac{2}{3}\left[\sigma_{33} - \frac{(\sigma_{11}+\sigma_{22})}{2}\right]d\lambda. \end{aligned} \tag{16}$$

The effective stress $(\bar{\sigma})$ and strain increment $(d\bar{\varepsilon})$ are given by,

$$\bar{\sigma} = \frac{1}{\sqrt{2}}[(\sigma_{22}-\sigma_{33})^2 + (\sigma_{33}-\sigma_{11})^2 + (\sigma_{11}-\sigma_{22})^2]^{1/2}, \tag{17}$$

$$d\bar{\varepsilon} = \frac{\sqrt{2}}{3}[(d\varepsilon_{11}-d\varepsilon_{22})^2 + (d\varepsilon_{22}-d\varepsilon_{33})^2 + (d\varepsilon_{33}-d\varepsilon_{11})^2]^{1/2} \tag{18}$$

Substituting the values of $d\varepsilon_{11}$, $d\varepsilon_{22}$ and $d\varepsilon_{33}$ from Eqs. (16) into Eq. (18) and using Eq. (17), we obtain,

$$d\bar{\varepsilon} = \frac{2}{3}\bar{\sigma}\, d\lambda. \tag{19}$$

From Eqs. (16) and (19) we get the strain increments

$$\begin{aligned} d\varepsilon_{11} &= \frac{d\bar{\varepsilon}}{\bar{\sigma}}\left[\sigma_{11} - \frac{(\sigma_{22}+\sigma_{33})}{2}\right], \\ d\varepsilon_{22} &= \frac{d\bar{\varepsilon}}{\bar{\sigma}}\left[\sigma_{22} - \frac{(\sigma_{11}+\sigma_{33})}{2}\right], \\ d\varepsilon_{33} &= \frac{d\bar{\varepsilon}}{\bar{\sigma}}\left[\sigma_{33} - \frac{(\sigma_{11}+\sigma_{22})}{2}\right]. \end{aligned} \tag{20}$$

On integrating the above set of equations (Eqs. (20)), one gets the strain rates,

$$\begin{aligned} \dot{\varepsilon}_{11} &= \frac{\dot{\bar{\varepsilon}}}{2\bar{\sigma}}[2\sigma_{11} - \sigma_{22} - \sigma_{33}], \\ \dot{\varepsilon}_{22} &= \frac{\dot{\bar{\varepsilon}}}{2\bar{\sigma}}[2\sigma_{22} - \sigma_{11} - \sigma_{33}], \\ \dot{\varepsilon}_{33} &= \frac{\dot{\bar{\varepsilon}}}{2\bar{\sigma}}[2\sigma_{33} - \sigma_{11} - \sigma_{22}]. \end{aligned} \tag{21}$$

Let A and A_0 denote the areas of transverse section of the disc element with outer radii r and b, respectively, but with the same inner radius a. The values of A and A_0 may be expressed as,

$$\left\{\begin{aligned} A &= \int_a^r h\,dr \\ A_0 &= \int_a^b h\,dr \end{aligned}\right\}. \tag{22}$$

The polar moment of area I and I_0 of these disc elements, with outer radii respectively as r and b but with the same inner radius a, is given by

$$\left\{\begin{aligned} I &= \int_a^r hr^2\,dr \\ I_0 &= \int_a^b hr^2\,dr \end{aligned}\right\}. \tag{23}$$

The average tangential stress in the disc $(\sigma_{\theta av})$ is

$$\sigma_{\theta av} = \frac{1}{A_0}\int_a^b h\sigma_\theta\, dr. \tag{24}$$

The set of constitutive equations (Eq. (21)) for creep in an isotropic composite material under biaxial state of stress (*i.e.* $\sigma_Z = 0$) takes the following form when the reference frame is along the principal directions r, θ and z [15]:

$$\begin{aligned} \dot{\varepsilon}_r &= \frac{\dot{\bar{\varepsilon}}}{2\bar{\sigma}}[2\sigma_r - \sigma_\theta], \\ \dot{\varepsilon}_\theta &= \frac{\dot{\bar{\varepsilon}}}{2\bar{\sigma}}[2\sigma_\theta - \sigma_r], \\ \dot{\varepsilon}_z &= \frac{\dot{\bar{\varepsilon}}}{2\bar{\sigma}}[-\sigma_r - \sigma_\theta], \end{aligned} \tag{25}$$

where $\dot{\varepsilon}_r, \dot{\varepsilon}_\theta, \dot{\varepsilon}_z$ and $\sigma_r, \sigma_\theta, \sigma_z$ are, respectively, the strain rates and the stresses in r, θ and z directions, as indicated by respective subscripts.

The effective stress $(\bar{\sigma})$, given by Eq. (17), in a rotating disc under biaxial state of stress may be expressed as,

$$\bar{\sigma} = \frac{1}{\sqrt{2}}\left[{\sigma_\theta}^2 + {\sigma_r}^2 + (\sigma_r - \sigma_\theta)^2\right]^{1/2}. \tag{26}$$

Substituting the value of $\dot{\bar{\varepsilon}}$ from Eq. (10) and $\bar{\sigma}$ from Eq. (26) into the first equation amongst set of equations in Eq. (25), the radial strain rate becomes

$$\dot{\varepsilon}_r = \frac{d\dot{u}_r}{dr} = \frac{[2x(r)-1]}{2[\{x(r)\}^2 - x(r)+1)]^{1/2}}\left[M(r)\{\overline{\sigma} - \sigma_0(r)\}\right]^n \tag{27}$$

where $x = \sigma_r/\sigma_\theta$ is the ratio of radial and tangential stresses, u is the radial deformation and $\dot{u}_r = du/dt$ is the radial deformation rate.

Similarly, the second equation of Eq. (25), yields the tangential strain rate,

$$\dot{\varepsilon}_\theta = \frac{\dot{u}_r}{r} = \frac{[2-x(r)]}{2[\{x(r)\}^2 - x(r)+1)]^{1/2}}\left[M(r)\{\overline{\sigma} - \sigma_0(r)\}\right]^n . \tag{28}$$

Dividing Eq. (27) by Eq. (28) and integrating the resulting equation between limits a to r, we get

$$\dot{u}_r = \dot{u}_a \exp\left[\int_a^r \frac{\phi(r)}{r}dr\right], \tag{29}$$

where $\dot{u}_a$ is the radial deformation rate at the inner radius and $\phi(r) = \dfrac{[2x(r)-1]}{[2-x(r)]}$.

Substituting $\dot{u}_r$ from Eq. (29) into Eq. (28), we get,

$$\frac{\dot{u}_a}{r}\exp\left[\int_a^r \frac{\phi(r)}{r}\right]dr = \frac{[2-x(r)]\left[M(r)\{\overline{\sigma} - \sigma_0(r)\}\right]^n}{2[\{x(r)\}^2 - x(r)+1)]^{1/2}} .$$

Simplifying the above equation, the tangential stress (σ_θ) is obtained as

$$\sigma_\theta = \frac{\dot{u}_a^{1/n}\psi_1(r)}{M(r)} + \psi_2(r), \tag{30}$$

where

$$\psi_1(r) = \frac{\psi(r)^{1/n}}{[\{x(r)\}^2 - x(r)+1)]^{1/2}},$$
$$\psi_2(r) = \frac{\sigma_0(r)}{[\{x(r)\}^2 - x(r)+1)]^{1/2}}, \tag{31}$$

and,

$$\psi(r) = \frac{2[\{x(r)\}^2 - x(r)+1)]^{1/2}}{r[2-x(r)]}\exp\left(\int_a^r \frac{\phi(r)}{r}dr\right). \tag{32}$$

Considering the equilibrium of forces acting on an element of the disc having varying thickness, the force equilibrium equation may be written as [18, 42]

$$\frac{d}{dr}[h(r)r\sigma_r] - h(r)\sigma_\theta + \rho(r)\omega^2 r^2 h(r) = 0 \tag{33}$$

where $\rho(r)$ is the density of composite disc.

It is assumed that the disc is connected to the shaft by means of splines where small axial movement is permitted. Therefore, a free-free condition applies [16], *i.e.*

$$\sigma_r = 0 \text{ at } r = a \text{ and } \sigma_r = 0 \text{ at } r = b . \tag{34}$$

Integrating Eq. (33) between limits a to b under the imposed boundary conditions given in Eq. (34), we get,

$$\int_a^b h(r)\sigma_\theta\, dr = \omega^2\left[A_\rho I_0 - B_\rho\left(\frac{(h_b+2cb)(b^4-a^4)}{4} - \frac{2c(b^5-a^5)}{5}\right)\right]. \tag{35}$$

Multiplying Eq. (30) by $h(r)dr$ and integrating the resulting equation between limits a to b, we get

$$\dot{u}_a^{1/n} = \frac{1}{\int_a^b \frac{h(r)\psi_1(r)}{M(r)}dr}\left[A_0\sigma_{\theta av} - \int_a^b h(r)\psi_2(r)dr\right]. \tag{36}$$

Dividing Eq. (35) by A_0 and noting Eq. (24), we get

$$\sigma_{\theta av} = \frac{1}{A_0}\int_a^b h(r)\sigma_\theta\, dr = \frac{\omega^2}{A_0}\left[A_\rho I_0 - B_\rho\left(\frac{(h_b+2cb)(b^4-a^4)}{4} - \frac{2c(b^5-a^5)}{5}\right)\right]$$

Knowing $\sigma_{\theta av}$, the tangential stress (σ_θ) is obtained after substituting the value of $\dot{u}_a^{1/n}$ from Eq. (36) into Eq. (30) as follows:

$$\sigma_\theta = \frac{\psi_1(r)\left[A_0\,\sigma_{\theta av} - \int_a^b h(r)\psi_2(r)dr\right]}{M(r)\int_a^b \frac{h(r)\psi_1(r)}{M(r)}dr} + \psi_2(r) . \tag{37}$$

Integrating Eq. (33) between limits a to r, the radial stress is obtained as

$$\sigma_r = \frac{1}{r\,h(r)}\left[\int_a^r h(r)\sigma_\theta dr - \omega^2 A_\rho I - \omega^2 B_\rho\left(\frac{(h_b+2cb)(r^4-a^4)}{4} - \frac{2c(r^5-a^5)}{5}\right)\right]. \tag{38}$$

The tangential stress (σ_θ) and the radial stress (σ_r) at any point in the composite disc are determined from Eqs. (37) and (38) respectively. Using these values, the strain rates $\dot{\varepsilon}_r$ and $\dot{\varepsilon}_\theta$ are calculated, respectively, from Eqs. (27) and (28).

7. Numerical computations

Following the procedure described in Section 6, the stresses and strain rates in the disc are estimated through an iterative numerical scheme shown in Fig. 3. The iteration is continued untill the process converges and yields the values of stresses at different points of the radius grid. For rapid convergence 75% of the value of σ_θ obtained in the current iteration has been mixed with 25% of the value of σ_θ obtained in the previous iteration and this modified value is used in the next iteration.

8. Results and discussions

A computer code, based on the mathematical formulation presented in Section 6, has been developed to obtain the distribution of stresses and steady state creep rates in various FGM discs having the same average SiCp content. For comparison, the results have also been obtained for a non-FGM disc having average SiCp content equal to that in FGM discs but distributed uniformly.

8.1 Validation

Before discussing the results obtained in this study, it is necessary to check the validity of analysis carried out and the software developed. For this purpose, the radial and tangential creep strains have been computed in a rotating steel disc by following the current analytical procedure. The results obtained are compared with the available experimental results for a steel disc [43]. The operating conditions, dimensions and creep parameters used for the steel disc are reported in Table 2.

To estimate the values of parameters M and σ_0 for a steel disc, the creep law given by Eq. (10) is integrated between limits of t from 0 to t to give

$$\bar{\varepsilon} = [M(\bar{\sigma} - \sigma_0)]^n \int_0^t f(t)dt\,, \tag{39}$$

where $\bar{\varepsilon}$ is the effective strain and $f(t)$ is function of time t.

Similar to the work of Wahl et al. [43], the function $f(t)$ is assumed to be unity during the validation process. Wahl et al. [43] observed that for steel disc the average strain at the end of 180 *hrs* and a mean stress $(\bar{\sigma})$ = 25,150 *psi* is 0.0109 *in/in,* whereas at a mean stress $(\bar{\sigma})$ = 29,450 *psi*, the strain observed is 0.029 *in/in.* Using the above reported values of stress and strain in Eq. (39), the creep parameters M and σ_0 for steel disc are estimated as 2.05 X 10^{-4} $s^{-1/5}/MPa$ and 35.98 *MPa*. These parameters have been used in the developed computer code to obtain the distribution of tangential and radial creep strains in the steel disc. Fig. 4 shows a good agreement between the results obtained by the procedure outlined in this study and the available experimental results for steel disc [43], which validates the analysis carried out and the software developed in this study.

ITER = Iteration no.

$E_{RR} = \dfrac{[\sigma_\theta]_{ITER} - [\sigma_\theta]_{ITER-1}}{[\sigma]_{ITER-1}}$

h = Limiting Value of ERR (=0.01)

ITM = Maximum no. of iteration = 50

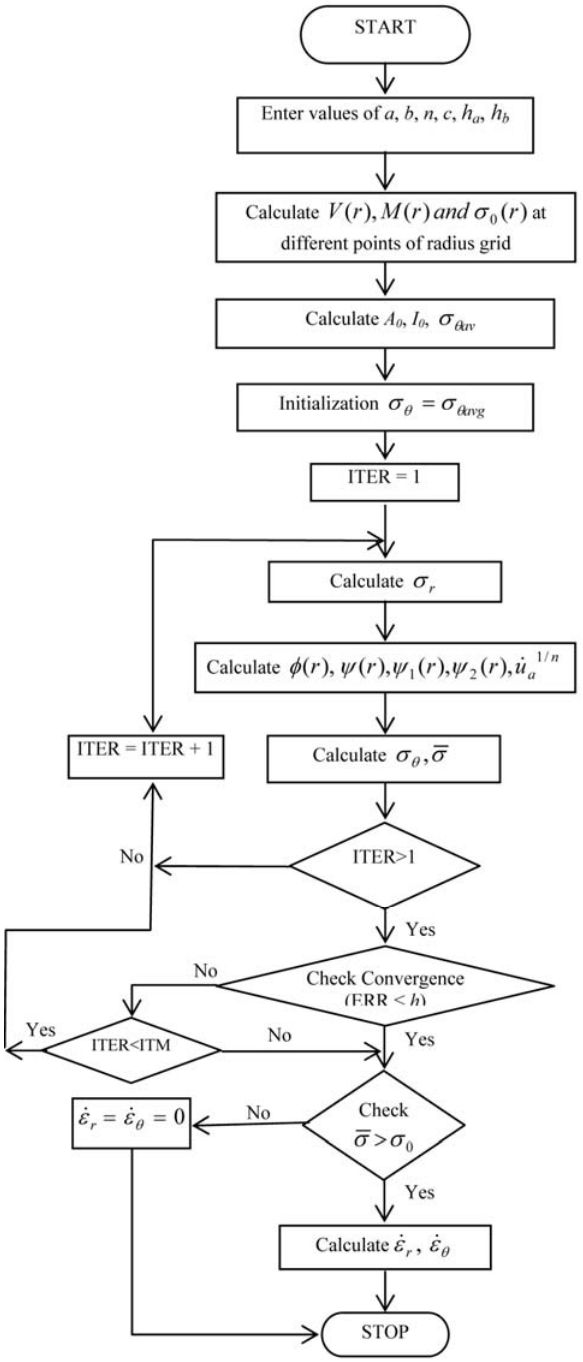

Fig. 3. Numerical scheme of computation.

Table 2. Parameters and operating conditions for steel disc.

Parameters for steel disc	Density of disc material (ρ) = 7,823.18 kg/m^3 Disc radius: a = 31.75 mm, b = 152.4 mm Disc Thickness: t = 25.4 mm Stress exponent: n = 5 Creep parameters: $M = 2.05 \times 10^{-4}\ s^{-1/5}/MPa$ σ_0 = 35.98 MPa
Operating conditions	Disc rpm = 15,000 Operating temperature = 810.78 K Creep duration = 180 hrs

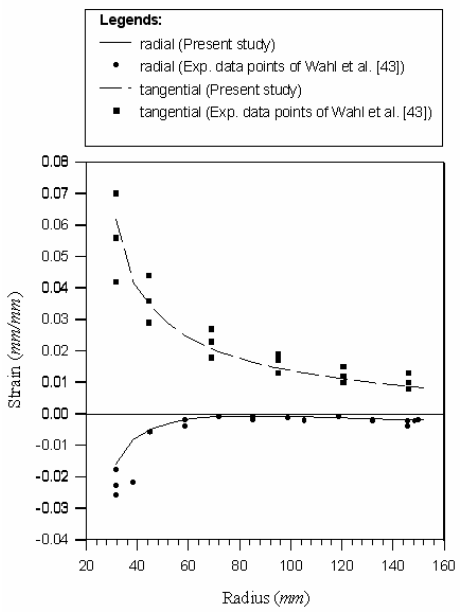

Fig. 4. Comparison of theoretical (Present Study) and experimental [43] strains in the steel disc (Disc rpm = 15000, Creep duration 180 hrs).

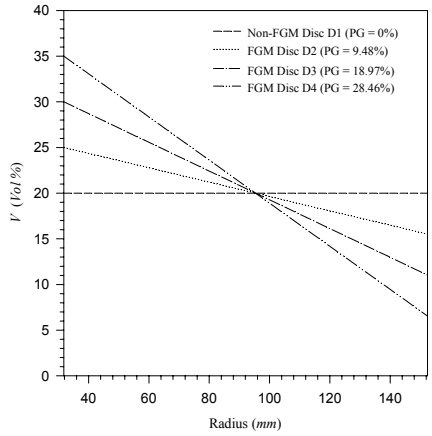

Fig. 5. Variation of particle content in composite discs.

8.2 Variation of creep parameters

Fig. 5 shows the distribution of reinforcement (SiCp) in various discs used in this study (refer to Table 3).

The SiCp content decreases linearly from the inner to the outer radius in FGM discs (D2-D4) while in uniform disc D1 (non-FGM disc) the content of SiCp remains 20 *vol %* over the entire radius. Figs. 6(a) and 6(b) show, respectively, the variation of creep parameters M and σ_0 with radial distance in the composite discs. The value of parameter M observed in FGM discs (D2-D4) increases with increasing radial distance. The increase observed in M is due to decrease in particle content $V(r)$ in the FGM discs (D2-D4) on moving from the inner to the outer radius, as evident from Eq. (11). With the increase in particle gradient (PG), defined as the difference of maxi-

Table 3. Description of rotating discs.

Disc (Notation)	Particle (SiCp) Content ($vol\%$)			Particle Gradient (PG) = V_{max} - V_{min} ($vol\%$)
	V_{max}	V_{min}	V_{av}	
Uniform/Non-FGM (D1)	20	20.00	20	0
FGM (D2)	25	15.52	20	9.48
FGM (D3)	30	11.03	20	18.97
FGM (D4)	35	6.54	20	28.46

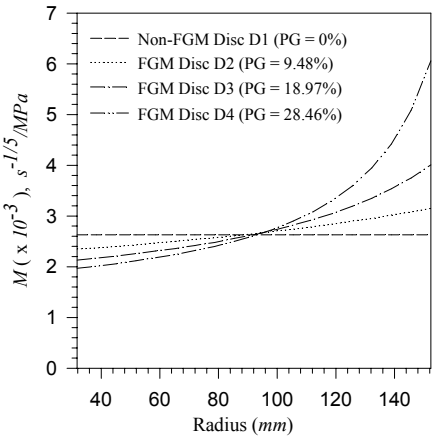

(a)

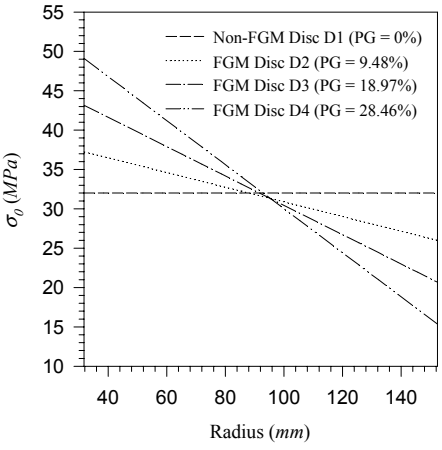

(b)

Fig. 6. Variation of creep parameters in composite discs.

mum and minimum particle content in the disc, the distribution of M becomes much steeper. On the other hand, the threshold stress (σ_0) shown in Fig. 6(b), decreases linearly with increasing radial distance as observed for the FGM disc (D2-D4). The threshold stress is higher in regions having more amount of SiCp compared to those having a relatively lesser amount of SiCp, which is also revealed from Eq. (12). Similar to the creep parameter M, the variation of σ_0 also becomes steeper with the increase in particle gradient in the FGM discs. Both the creep parameters, M and σ_0, observed in uniform disc (D1) remains constant due to uniform distribution of SiCp reinforcement (i.e. 20 *vol%* SiCp) over the entire disc.

8.3 Distribution of stresses and strain rates

The effect of particle gradient (PG) on creep behavior of uniform and FGM discs is shown in Figs. (7)-(8). The radial stress in all the discs, Fig. 7(a), increases from zero at inner radius, reaches maximum before dropping to zero again at the outer radius, under the imposed boundary conditions given in Eq. (34). By increasing PG in the disc, the radial stress is observed to increase over the entire disc.

The radial stress is highest in FGM disc D4 and lowest in uniform disc D1. The maximum value of radial stress in FGM discs D2, D3 and D4 is higher, respectively, by about 11%, 23% and 33%, when compared with those observed in uniform disc D1. As compared to uniform thickness disc D1, the radial stress in FGM discs D2, D3 and D4 is higher near the inner radius due to higher density, which causes the centrifugal force to increase. But toward the outer radius, in spite of lower density of FGM discs, the radial stress is higher in FGM discs than the uniform thickness disc D1 due to relatively lower thickness. Fig. 7(b) shows the variation of tangential stress in different composite discs. By increasing PG in the FGM disc the tangential stress increases near the inner radius but decreases towards the outer radius when compared with distribution of tangential stress in uniform disc D1. The distribution of tangential stress exhibits a crossover at a radial distance of around 78.67 *mm*, Fig. 7(b). In the FGM discs (D2-D4), the higher and lower density of the disc, respectively, near the inner and outer radii, compared to the density of uniform disc D1, are responsible for relatively higher and lower tangential stresses near the inner and outer radii, as revealed from equilibrium Eq. (38). As compared to uniform disc D1, the maximum values of tangential stress in FGM discs D2, D3 and D4 are higher by about 10%, 20% and 30% respectively. The variation of effective stress with radial distance for different discs, as shown in Fig. 7(c), is similar those observed for tangential stress in Fig. 7(b).

The strain rates, tangential as well as radial, decrease significantly with increasing PG in the disc as evident from Figs. 8(a) and 8(b). Though, near the inner radius the tangential stress in the FGM discs is higher than the uniform disc D1 due to higher density, but the FGM discs exhibit lower tangential

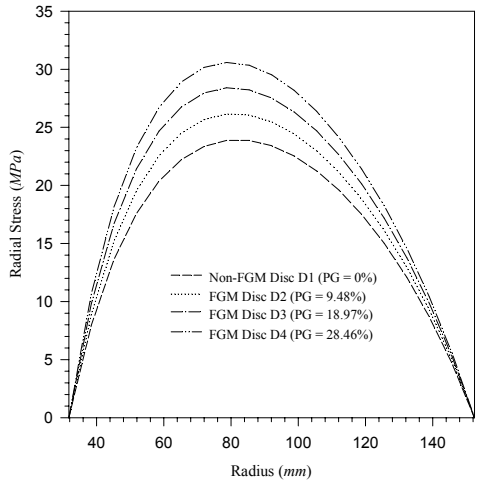

Fig. 7(a) Effect of particle gradient on radial stress.

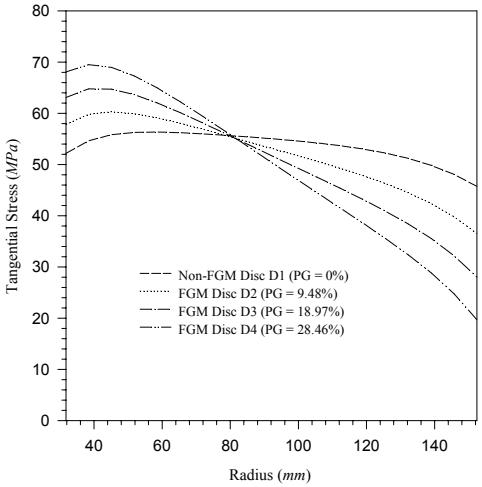

Fig. 7(b) Effect of particle gradient on tangential stress.

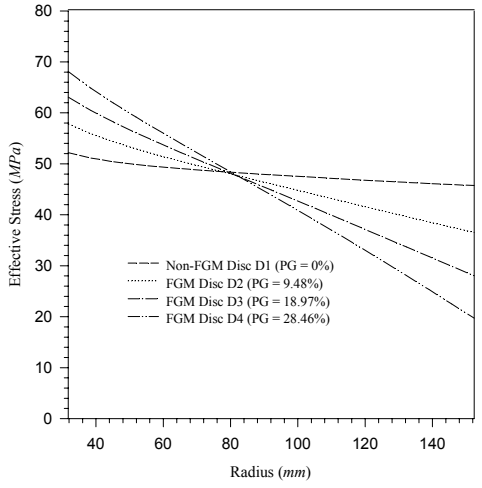

Fig. 7(c) Effect of particle gradient on effective stress.

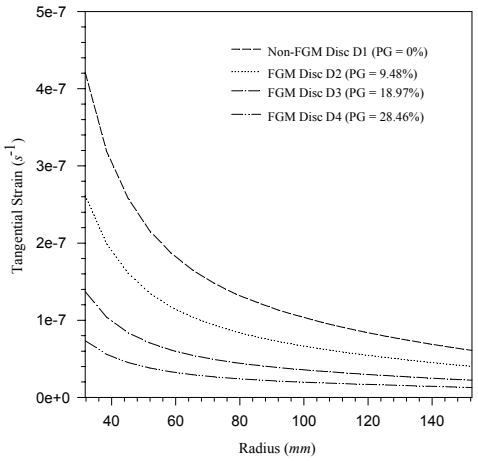

Fig. 8(a) Effect of particle gradient on tangential strain rate.

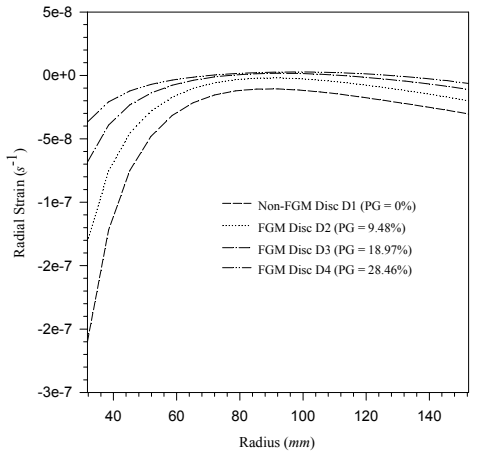

Fig. 8(b) Effect of particle gradient on radial strain rate.

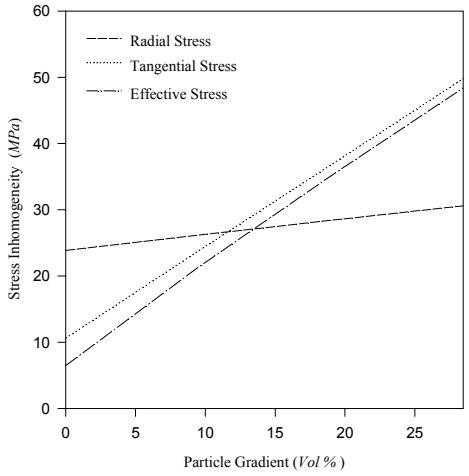

Fig. 9(a) Effect of particle gradient on stress inhomogeneity.

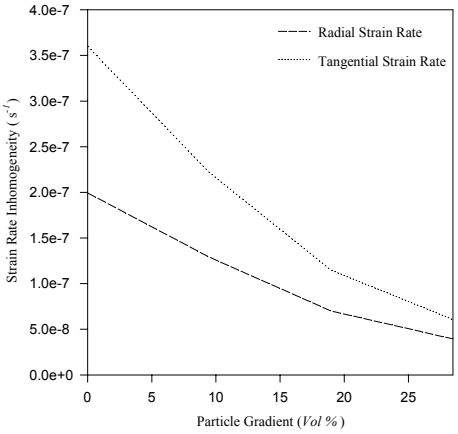

Fig. 9(b) Effect of particle gradient on strain rate inhomogeneity.

creep rates near the inner radius than the uniform disc D1. It is attributed to lower and higher values of parameters M and σ_0, Figs. 6(a)-(b), near the inner radius of FGM discs (D2-D4) than the uniform disc D1. On the other hand, the tangential strain rate near the outer radius of the FGM discs (D2-D4) is lower than the uniform disc D1, due to lower tangential stress, Fig. 7(b), caused by the lower density of FGM discs towards the outer radius. At the outer radius, the increase and decrease in parameters M and σ_0, respectively, with increasing PG, Figs. 6(a)-(b), could not dominate the decrease in tangential stress. The decrease in tangential strain rate is more at the inner radius than that observed towards the outer radius. The effect of increasing the PG on the radial strain rate, Fig. 8(b), is similar to that observed for tangential strain rate in Fig. 8(a). By increasing the PG beyond 9.48%, the nature of radial strain rate, which is generally compressive, becomes tensile in the middle of the disc, as noticed for FGM discs D3 and D4. The maximum tensile radial strain rate is observed somewhere in the middle of FGM disc D4, which possesses maximum PG.

It is also evident from Figs. 8(a) and 8(b) that besides decrease in strain rates with increasing PG, the distribution of strain rates becomes relatively more uniform. Therefore, the FGM disc having higher PG will have less chances of distortion.

The stress inhomogeneity, defined as the difference of maximum and minimum values of stress, increases with increasing particle gradient as shown in Fig. 9(a). For 1% increase in particle gradient in the FGM disc, the inhomogeneity in radial, tangential and effective stress increases by about 0.23 *MPa*, 1.37 *MPa* and 1.47 *MPa* respectively. Unlike stress inhomogeneity, the tangential as well as radial strain rate inhomogeneity in the disc decreases significantly with increasing particle gradient as shown in Fig. 9(b). The decrease is steeper up to about 18% particle gradient followed by a relatively lower decrease with further increase in particle gradient. The decrease observed in tangential strain rate inhomogeneity is relatively higher than that observed in radial strain rate.

9. Conclusions

The study carried out has led to the following conclusions:

- In the presence of particle gradient in a rotating disc, the

tangential stress increases near the inner radius but decreases near the outer radius.

- The radial stress in a rotating disc increases everywhere with the increase in particle gradient.
- In the FGM discs with linearly decreasing particle content from the inner to the outer radius, the steady state creep response in terms of strain rates is superior to that observed in a disc containing uniform distribution of reinforcement, when both the discs have the same average amount of reinforcement.
- By employing higher particle gradient in the FGM disc, the distribution of strain rates in the disc becomes relatively more uniform.

References

[1] V. K. Gupta, S. B. Singh, H. N. Chandrawat and S. Ray, Modeling of creep behavior of a rotating disc in the presence of both composition and thermal gradients, *Journal of Engineering Materials and Technology*, 127 (2005) 97-105.

[2] M. H. Hojjati and A. Hassani, Theoretical and numerical analysis of rotating discs of non-uniform thickness and density, *International Journal of Pressure Vessels and Piping* 85 (10) (2008) 694-700.

[3] S. B. Singh and S. Ray, Modeling the anisotropy and creep in orthotropic aluminum-silicon carbide composite rotating disc, *Mechanics of Materials* 34 (2002) 363-372.

[4] L. H. You, X. Y. You, J. J. Zhang and J. Li, On rotating circular disks with varying material properties, *Zeitschrift fur angewandte Mathematik und Physik* 58 (2007) 1068-1084.

[5] B. Farshi and J. Bidabadi, Optimum design of inhomogeneous rotating discs under secondary creep, *International Journal of Pressure Vessels and Piping* 85 (2008) 507-515.

[6] V. K. Gupta, N. Kwatra and S. Ray, Artificial neural network modeling of creep behavior in a rotating composite disc, *Engineering Computations: International Journal for Computer-Aided Engineering and Software* 24 (2) (2007) 151-164.

[7] B. Farshi, H. Jahed and A. Mehrabian, Optimum design of inhomogeneous non-uniform rotating discs, *Computers and Structures* 82 (2004) 773-779.

[8] M. Laskaj, B. Murphy and K. Houngan, Improving the efficiency of cooling the front disc brake on a V8 racing car, *Project report*, Monash University, Melbourne (1999).

[9] M. Bayat, M. Saleem, B. B. Sahari, A. M. S. Hakouda and E. Mahdi, Analysis of functionally graded rotating disks with variable thickness, *Mechanics Research Communications* 35 (2008) 283-309.

[10] T. G. Nieh, Creep rupture of a silicon carbide reinforced aluminum composite, *Metallurgical Transactions* 15A (1984) 139-146.

[11] T. G. Nieh, K. Xia and T. G. Langdon, Mechanical properties of discontinuous SiC reinforced aluminium composites at elevated temperatures, *Journal of Engineering Materials and Technology* 110 (1988) 77-82.

[12] J. N. Reddy, Analysis of functionally graded plates, *International Journal of Numerical Method Engineering* 47 (2000) 663-684.

[13] S. Suresh and A. Mortensen, Fundamentals of Functionally Graded Materials, processing and thermomechanical behavior of graded metals and metals-ceramic composites, *IOM Communications Limited*, London (1998).

[14] S. B. Singh and S. Ray, Steady state creep behavior in an isotropic functionally graded material rotating disc of Al-SiC composite, *Metallurgical and Materials Transactions* 32 (7) (2001) 1679-1685.

[15] V. K. Gupta, S. B. Singh, H. N. Chandrawat and S. Ray, Steady state creep and material parameters in a rotating disc of Al-SiC_p composite, *European Journal of Mechanics A/Solids* 23 (2004) 335-344.

[16] M. N. Bayat, M. Saleem, B. B. Sahari, A. M. S. Hamouda and E. Mahdi, Thermo elastic analysis of a functionally graded rotating disk with small and large deflections, *Thin-Walled Structures* 45 (2007) 677-691.

[17] S. A. H. Kordkheili and R. Naghdabadi, Thermo elastic analysis of a functionally graded rotating disk, *Composite Structures* 79 (4) (2007) 508-516.

[18] N. S. Bhatnagar, P. S. Kulkarni and V. K. Arya, Steady-state creep of orthotropic rotating disks of variable thickness, *Nuclear Engineering and Design* 91 (2) (1986) 121-144.

[19] A. N. Eraslan and Y. Orcan, Elastic-plastic deformation of a rotating disk of exponentially varying thickness, *Mechanics of Materials* 34 (2002) 423-432.

[20] Y. Orcan and A. N. Eraslan, Elastic-plastic stresses in linearly hardening rotating solid disks of variable thickness, *Mechanics Research Communications* 29 (2002) 269-281.

[21] H. Jahed, B. Farshi and J. Bidabadi, Minimum weight design of inhomogeneous rotating discs, *International Journal of Pressure Vessels and Piping* 82 (2005) 35-41.

[22] S. K Gupta, S. Sharma and S. Pathak, Creep transition in a thin rotating disc having variable thickness and variable density, *Indian Journal of Pure Applied Mathematics* 31 (10) (2000) 1235-1248.

[23] D. Deepak, V. K. Gupta and A. K. Dham, Steady state creep in a rotating composite disc of variable thickness, *International Journal of Materials Research* 101 (2010) 780-786.

[24] T. W. Clyne and P. J. Withers, *An Introduction to Metal Matrix Composites*, Cambridge Univ. Press, Cambridge, UK, (1993) 479.

[25] *Metals Handbook* (*vol. 2*), American Society of Metals, 9th Ed., Metals Park, Ohio, USA, (1978) 714.

[26] Z. Y. Ma and S. C. Tjong, Creep deformation characteristics of discontinuously reinforced aluminium matrix composites, *Composites Science and Technology* 61 (5) (2001) 771-786.

[27] S. C. Tjong and Z. Y. Ma, Microstructural and mechanical characteristics in situ metal matrix composites, *Materials Science and Engineering* 29 (2000) 49-113.

[28] G. Gonzalez-Doncel and O. D. Sherby, High temperature

creep behavior of metal matrix aluminium-SiC composites, *Acta Metallurgica et Materialia* 41 (10) (1993) 2797-2805.
[29] R. S. Mishra and A. B. Pandey, Some observation on the high-temperature creep behavior of 6061 Al-SiC composites, *Metallurgical Transactions* 21A (1990) 2089-2090.
[30] A. B. Pandey, R. S. Mishra and Y. R. Mahajan, Steady state creep behavior of silicon carbide particulate reinforced aluminium composites, *Acta Metallurgica et Materialia* 40 (1992) 2045-2052.
[31] A. B. Pandey, R. S. Mishra and Y. R. Mahajan, High-temperature creep of Al-TiB_2 particulate composites, *Materials Science and Engineering* 189A (1994) 95-104.
[32] J. Cadek, H. Oikawa and V. Sustek, Threshold creep behavior of discontinuous aluminium and aluminium alloy matrix composites: An Overview, *Materials Science and Engineering* A190 (1995) 9-21.
[33] Y. Li and T. G. Langdon, Creep behavior of an Al-6061 metal matrix composite reinforced with alumina particulates, *Acta Materialia* 45 (11) (1997) 4797-4806.
[34] Y. Li and T. G. Langdon, An examination of a substructure-invariant model for the creep of metal matrix composites, *Materials Science and Engineering* A265 (1999) 276-284.
[35] Y. Li and F. A. Mohamed, An investigation of creep behavior in an SiC-2124 Al composite, *Acta Materialia* 45 (11) (1997) 4775-4785.
[36] F. A. Mohamed, K. T. Park and E. J. Lavernia, Creep behavior of discontinuous SiC–Al composites, *Materials Science and Engineering* 150A (1992) 21-35.
[37] K. T. Park, E. J. Lavernia and F. A. Mohamed, High temperature creep of silicon carbide particulate reinforced aluminum, *Acta Metallurgica et Materialia*, 38 (11) (1990) 2149-2159.
[38] K. T. Park and F. A. Mohamed, Creep strengthening in a discontinuous SiC–Al composite, *Metallurgical and Materials Transactions* 26A (1995) 3119-3129.
[39] H. Yoshioka, Y. Suzumura, J. Cadek, S. J. Zhu and K. Milicka, Creep behavior of ODS aluminium reinforced by silicon carbide particulates: ODS Al–30 SiC_P composite, *Materials Science and Engineering* A248 (1) (1998) 65-72.
[40] R. Lagneborg and B. Bergman, The stress/creep behavior of precipitation-hardened alloys, *Metal Science* 10 (1) (1976) 20-28.
[41] V. Mises, Translation of Mechanik der festen koerper im plastisch-deformablem Zustrand Nachrichten von der koniglichen Gasellschaft der Wissenschaften, *Technical Memorandum 88488*, NASA, Washington DC (1986) 582-592.
[42] S. P. Timoshenko and J. N.Goodier, *Theory of Elasticity*, McGraw-Hill, Singapore (1970) 82.
[43] A. M. Wahl, G. O. Sankey, M. J. Manjoine and E. Shoemaker, Creep tests of rotating disks at elevated temperature and comparison with theory, *Journal of Applied Mechanics* 21 (1954) 225-235.

Dharmpal Deepak holds a Bachelors Degree in Mechanical Engineering from SLIET, Longowal (India) and Masters in Production Engineering from GNDEC, Ludhiana (India). Presently, he is working as an Assistant Professor in the Mechanical Engineering Department at RIEIT, Nawanshehr, India. He has number of publications in refereed Journals and Conferences. His main research area is Mechanics of Composite Materials.

V. K. Gupta received his Bachelors Degree in Mechanical Engineering from HBTI, Kanpur, (India) and Masters in Industrial Metallurgy from IIT Roorkee (India). He then obtained his Ph.D. in Mechanical Engineering from TIET, Patiala (India). Dr. Gupta is currently working as a Reader in Mechanical Engineering at UCoE, Punjabi University, Patiala, India. He has published thirty five plus research papers in refereed Journals and Conferences. His main research interests are Mechanics of Composite Materials, Fatigue Behavior of PVD Coated Steels Components and Hard Part Turning.

Dr. Ashok K. Dham holds a Ph.D. in Theoretical Physics from Punjabi University, Patiala, India. Presently, he is working as Professor of Physics at Punjabi University, Patiala (India). His main areas of research are Intermolecular Forces, Atomic and Molecular Physics, and Computational Physics. He has published thirty plus research papers in the leading related International/National Journals of repute, and has presented papers in about twelve International Conferences on Intermolecular Forces/Transport Properties. He has spent six years at University of Western Ontario (Canada) and a year and half at University of Waterloo (Canada) on sabbaticals.